

https://doi.org/10.1070/QEL16945

Experimental studies of 1.5–1.6 μm high-power asymmetric-waveguide multimode lasers

O.O. Bagaeva, A.I. Danilov, A.V. Ivanov, V.D. Kurnosov, K.V. Kurnosov, Yu.V. Kurnyavko, A.A. Marmalyuk, V.I. Romantsevich, V.A. Simakov, R.V. Chernov

Abstract. **The current–voltage, light–current, and spectral characteristics of high-power multimode semiconductor lasers emitting at wavelengths of 1.5–1.6 μm are studied experimentally. It is shown that the cw output power of a C-mount laser with a cavity length of 2.6 mm and a mesa-stripe contact width of 100 μm exceeds 4 W at a pump power of 15 A. The output power in a pulsed regime amounts to 20 W at a pulse duration of 100 ns, a pulse repetition rate of 5 kHz, and a pump current no higher than 80 A. The dependences of the laser wavelength and spectral width on the pump current are presented. The current–voltage and light–current characteristics, as well as the characteristic temperatures of the lasers, are calculated.**

Keywords: *multimode lasers; current–voltage, light–current and spectral characteristics; wavelength 1.5–1.6 μm; radiation spectral width.*

1. Introduction

Interest in high-power laser diodes (LDs) emitting in the wavelength range of 1400–1600 nm is explained by their application in open communication lines, as pump sources for erbium-doped fibre-optic amplifiers, in medicine, in environment-monitoring systems, and in spectroscopy of industrial gases. It is believed that radiation in this wavelength range is eye safe.

The maximum cw output power of an InGaAsP/InP laser diode with an aperture of 200 μm and wavelength $\lambda = 1.5$ μm was achieved in 1996 [1] to be 4.6 W.

The InGaAsP/InP laser heterostructures (HS's) with two strained quantum wells ($\lambda = 1.3$–1.55 μm) grown in [2] by vapour-phase epitaxy emitted a cw optical power of 2.4 W at 20 °C and a stripe contact width of 100 μm. The authors of [3] achieved the maximum cw power of 4.5 W at a pump current of 12 A, a cavity length of 2.5 mm, a temperature of 20 °C, and an aperture of 95 μm. The pulsed power was 16.5 W at a pump current 80 A and a cavity length of 2 mm.

In [4], it was shown that an LD with one quantum well can emit cw optical power of 2.5 W at a pump current of 5 A and a stripe contact of 0.1 × 1.5 mm. Within the temperature range of 10–70 °C, the characteristic temperatures for the threshold current density and the differential efficiency were 90 and 325 K, respectively. No LD degradation was observed during tests for more than 4000 hours at a pump current of 5 A and a temperature of 40 °C. Studies of LDs made of three AlInGaAs/InP HS's with waveguide thicknesses and band gap widths of 0.3 μm and 1.0 eV, 1.5 μm and 1.0 eV, and 1.5 μm and 1.12 eV showed that the pulsed output powers were 2 W for the first HS, 6 W for the second, and 9.5 W for the third [5]. Therefore, optimisation of the geometry of the waveguide layer of the HS strongly affects the characteristics of LDs emitting in the range of 1.5–1.6 μm.

High-power multimode lasers based on AlInGaAs/InP quantum well heterostructures with an ultra-narrow waveguide and a 100-μm stripe contact demonstrated room-temperature output optical powers exceeding 4 W in a cw regime and exceeding 20 W in a pulsed regime [6]. The influence of the thickness of waveguide layers on the output characteristics of LDs was studied in [7]. It was shown that the internal optical losses are 2.2 cm^{-1} in a wide waveguide and 3.5 cm^{-1} in a narrow waveguide. Lasers with a wide waveguide can emit output pulsed powers of 16 W, while the output pulsed power of lasers with a narrow waveguide may amount only to 10 W. In the cw mode, the output power of a narrow-waveguide laser was 3.8 W at a pump current of 13 A, while the output power of the wide-waveguide laser was only 3 W at a current of 11 A. Wide-waveguide lasers were shown to have a higher differential efficiency η at a relatively small excess over the threshold current, while narrow-waveguide lasers retain η to higher pump currents and are preferable for achieving maximum powers. The characteristic temperature for the threshold current density in the case of wide-waveguide lasers was 45–50 K, which is somewhat lower than that for narrow-waveguide lasers (60–65 K). The characteristic temperature for the differential quantum efficiency for wide-waveguide lasers was 120–140 K, i.e., lower than that for narrow-waveguide lasers (180–200 K). A review on high-power LDs is presented in [8].

In the present work, we experimentally and theoretically study 1.5–1.6-μm high-power multimode lasers with a strongly asymmetric waveguide. The lasers were made of the same HS as the single-mode lasers in [9]. The difference consisted in the width of the mesa-stripe contact (100 μm instead of 3 μm) and in the dielectric used for the contact isolation (Si_3N_4 instead of ZnSe).

2. Characteristics of multimode lasers

We studied lasers with cavity lengths $L_c = 2.2$ and 2.6 mm. The cavity faces were coated with high-reflection (~100%)

O.O. Bagaeva, A.I. Danilov, A.V. Ivanov, V.D. Kurnosov, K.V. Kurnosov, Yu.V. Kurnyavko, A.A. Marmalyuk, V.I. Romantsevich, V.A. Simakov, R.V. Chernov Open Joint-Stock Company M.F. Stel'makh Polyus Research Institute, ul. Vvedenskogo 3, stroenie 1, 117342 Moscow, Russia; e-mail: webeks@mail.ru

Received 28 December 2019
Kvantovaya Elektronika **49** (7) 649–652 (2019)
Translated by M.N. Basieva

and antireflection (5%) coatings. The LD characteristics were measured from the cavity face with the 5% reflectivity. The LDs were soldered active side down onto copper C-mounts ($5.5 \times 6 \times 7$ mm). An electronic stabilisation scheme was used to keep the C-mount temperature T constant within the range of 20–60 °C ($T = T_0 + \Delta T$, where $T_0 = 20$ °C and $\Delta T = 0, 10, 20, 30$, and 40 °C). The current–voltage and ligh–current characteristics (CVCs and LCCs, respectively) were measured at these fixed temperatures and a continuous pump current. To measure pulsed LCCs, the C-mounts were mounted on a heat sink 40 mm in diameter and 5 mm thick. The measurements were performed at room temperature, an electric pulse duration of 100 ns, and a pulse repetition rate of 5 kHz; we also measured the optical pulse duration, which was used to calculate the pulsed output power.

2.1. Current–voltage and light–current characteristics of LDs

The power of LDs with the cavity length $L_c = 2.6$ mm exceeded 4.2 W at a temperature of 20 °C and a pump current higher or equal to 15 A. The LDs with $L_c = 2.2$ and 2.6 mm at $T_0 = 20$ °C had approximately the same CVCs and LCCs. However, the LCC of the LD with $L_c = 2.2$ mm at $T = 60$ °C saturated at currents of 13–13.5 A, while the LCC of the LD with $L_c = 2.6$ mm exhibited no saturation up to currents exceeding 15 A. In this connection, hereinafter we present the results for the LD with the cavity length of 2.6 mm. Figure 1 shows the CVCs and LCCs for the LD with $L_c = 2.6$ mm operating in a cw regime at different heat-sink temperatures.

Figure 2 presents the experimental dependences of the pulsed power and the optical pulse duration on the pump current. At a pulsed pump current $I = 80$ A, the power exceeds 19.5 W. One can see from Fig. 2 that the optical pulse duration at low currents is smaller than 100 ns and increases to 120 ns at $I = 80$ A. This is explained by a delay between the optical and electric pulses at pump currents close to threshold values due to the finite time of the formation of the threshold population inversion in the LD, which leads to a decrease in the optical pulse duration. The increase in the optical pulse duration at high pump currents (after the electric pulse termination) is caused by the finite time of population inversion relaxation [10]. Experiments showed that the optical pulse duration of the LD with a symmetric wide waveguide is 120 ns at $I \approx 20$ A and increases to 150 ns at currents exceeding 80 A. In our case, this is caused by a considerable decrease in the p-waveguide thickness and in the time of the hole transport to the LD active region. Therefore, the pulsed LD power should be calculated using the optical pulse duration rather than the electric pulse duration.

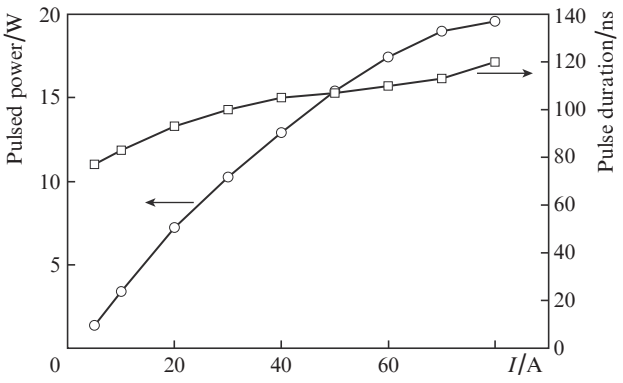

Figure 2. Experimentally measured dependences of the output power and the optical pulse duration on the pump current.

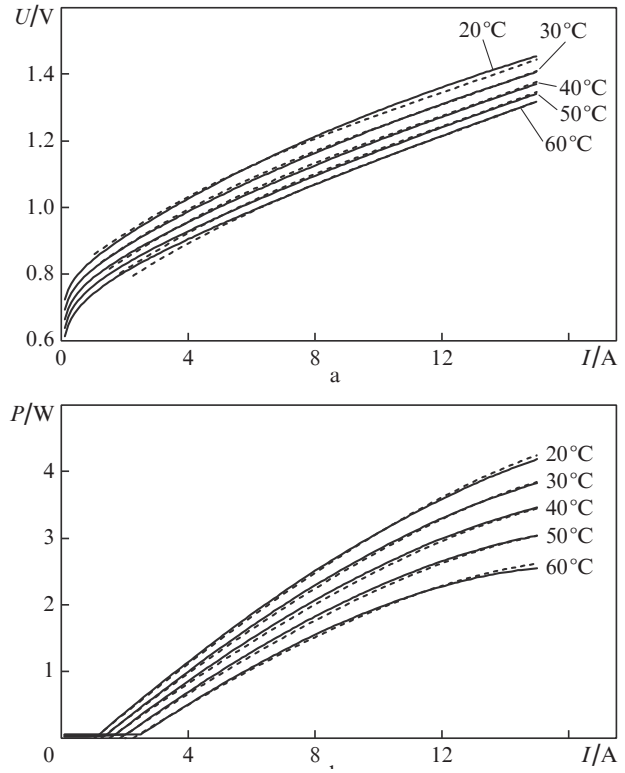

Figure 1. (Solid curves) Experimentally measured and (dashed curves) calculated (a) current–voltage and (b) light–current characteristics of the LD with a cavity length of 2.6 mm at different LD temperatures.

2.2. Differential resistance and differential efficiency

It is shown in [9, 11] that the differential LD resistance only slightly affects the lasing threshold and the differential efficiency but strongly affects the radiation power, i.e., the lower the differential resistance, the higher the maximum power.

Figure 3 presents the calculated dependences of the differential resistance R_d on the continuous pump current I for

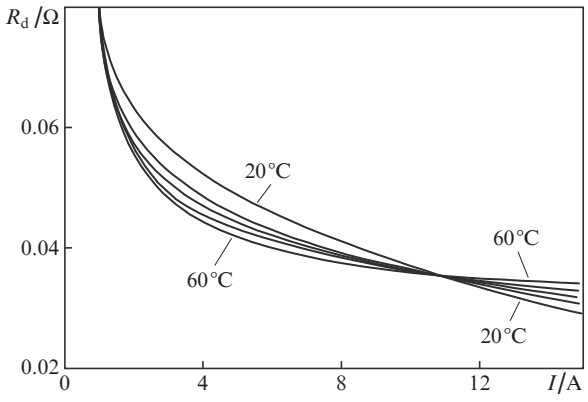

Figure 3. Dependences of the dynamic resistance R_d on the continuous pump current at heat-sink temperatures of 20–60 °C. The interval between the curves is 10 °C.

the LD with a cavity length of 2.6 mm in the temperature range of 20–60 °C. One can see that R_d depends on temperature and is ~0.03 Ω at $T = 20$ °C and a current of 15 A (pump current density 5.8 kA cm^{-2}), when the output power exceeds 4 W. Note that R_d for the LD with a stripe contact width of 3 μm at a pump current of 1.2 A was ~0.6 Ω at $T = 20$ °C, when the output power exceeded 0.3 W [9].

The resistance R_d decreases with increasing output power (pump current) [12], and the decrease rate depends on temperature. Analysis of the curves presented in Fig. 3 shows that the curve $R_d(I)$ for $T = 60$ °C lies below the curve for 20 °C at pump currents smaller than 11 A and above this curve at pump currents exceeding 11 A, i.e., the rate of change in the differential resistance with pump current in absolute terms decreases with increasing temperature. At the same time, the voltage at the LD at $T = 60$ °C is lower than at $T = 20$ °C.

Figure 4 shows the calculated dependences of the differential efficiency η of LCCs on the continuous pump current in the temperature range of 20–60 °C. Comparison of these dependences with the corresponding dependences from [9] shows that the values of η do not strongly differ from each other.

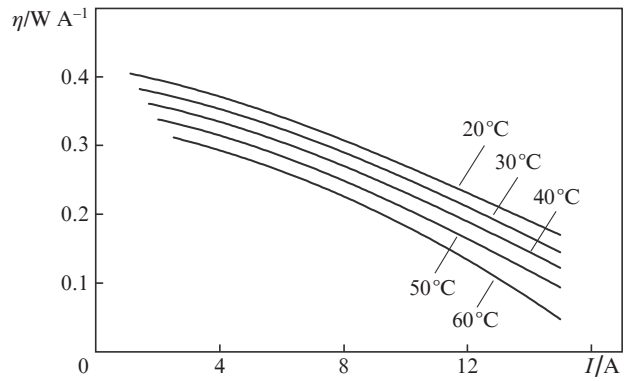

Figure 4. Dependences of the differential efficiency η of LCCs on the pump current at heat-sink temperatures of 20–60 °C. The interval between the curves is 10 °C.

2.3. Spectral characteristics of LDs

Figure 5 presents the experimental spectra of the LD operating in a pulsed pumping regime at pump currents of 5 and 80 A and a heat-sink temperature of 25 °C. Similar to the case of continuous pump current [9], the laser spectrum is considerably broader at the higher current (heating of the LD active region can be ignored in both cases). As is shown in [13], the increase in the spectral width is caused by nonlinear losses.

Figure 6 shows the measured dependences of the laser wavelength and the full width at half maximum (FWHM) of the laser spectrum on the pulsed pump current. Both the wavelength and the spectral width increase with increasing current; in particular, the laser wavelength increases almost linearly with a rate of 0.12 nm A^{-1}. The dependence of the spectral FWHM on the pulsed current has a character similar to the character of the dependence observed in [9].

3. Calculation of CVCs, LCCs, and characteristic temperatures of LDs

To perform these calculations, we will use the results of works [9, 14]. Let us write the voltage across the LD in the form

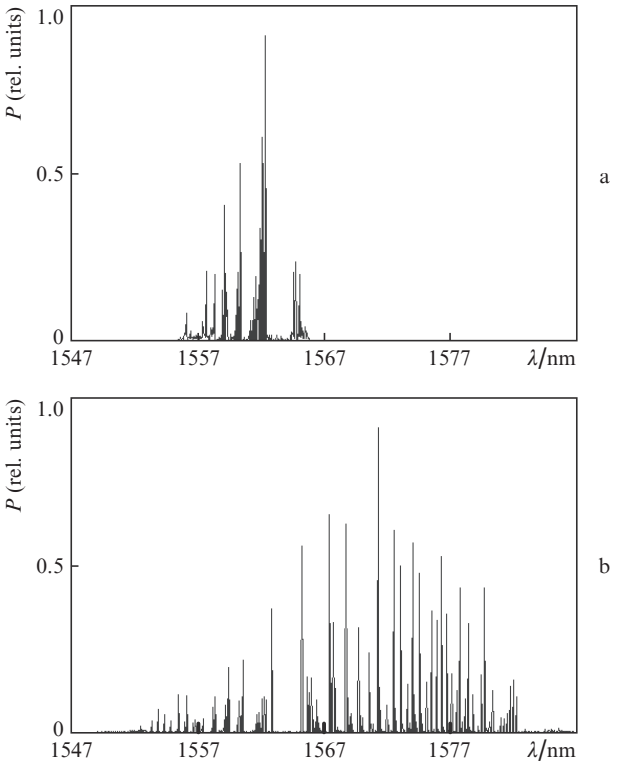

Figure 5. Experimentally measured spectra of an LD with a cavity length of 2.6 mm under pulsed pumping at pump currents of (a) 5 and (b) 80 A and a heat-sink temperature of 25 °C.

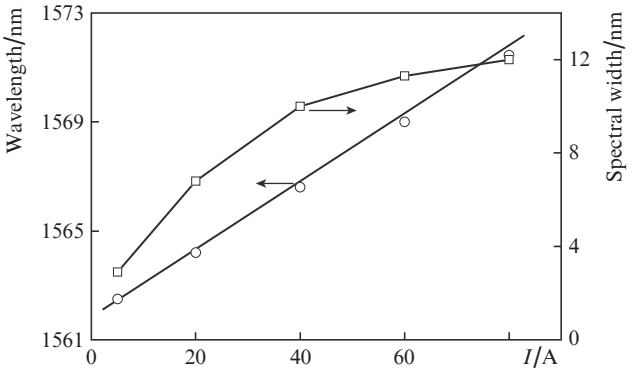

Figure 6. Experimentally measured dependences of the laser wavelength and the spectral FWHM on the pulsed pump current.

$$U(I, \Delta T_{LD}) = U_{cut}(\Delta T_{LD}) + IR_d(I). \quad (1)$$

Assume that the LD resistance $R_d(I)$ depends only on the pump current, while the cutoff voltage $U_{cut}(\Delta T_{LD})$ depends only on the active region heating ΔT_{LD}. In contrast to [9, 14], in which the temperature range was 20–40 °C, in the present work we consider the range of 20–60 °C, because of which we retain the second derivatives in the expansion of the $R_d(I)$ and $U_{cut}(\Delta T_{LD})$ functions in the Taylor series:

$$R_d(I) = R_{d0}(1 - dR_1 I + 0.5dR_2 I^2), \quad (2)$$

$$U_{cut}(\Delta T_{LD}) = U_{0cut}(1 - dU_1 \Delta T_{LD} + 0.5dU_2 \Delta T_{LD}^2), \quad (3)$$

where $U_{0\,\mathrm{cut}}$ is the cutoff voltage (linear approximation of the experimental CVC to the pump current tending to zero); $R_{\mathrm{d}0}$ is the dynamic resistance of the LD at $T = T_0$; and $\mathrm{d}R_1, \mathrm{d}R_2, \mathrm{d}U_1$, and $\mathrm{d}U_2$ are the first and second derivatives of the corresponding parameters.

The LCC was calculated by the formula

$$P = \eta_{\mathrm{th}}(I, P, \Delta T)[I - I_{\mathrm{th}}(I, P, \Delta T)]. \quad (4)$$

The dependences of the threshold current I_{th} and the differential efficiency at the lasing threshold η_{th} on the pump current, output power, and temperature are determined by the formulas

$$I_{\mathrm{th}}(I, P, \Delta T) = I_{\mathrm{th}\,0}\exp\left(\frac{\Delta T_{\mathrm{LD}}(I, P, \Delta T)}{T_I}\right), \quad (5)$$

$$\eta_{\mathrm{th}}(I, P, \Delta T) = \eta_{\mathrm{th}\,0}\exp\left(\frac{-\Delta T_{\mathrm{LD}}(I, P, \Delta T)}{T_P}\right), \quad (6)$$

where $I_{\mathrm{th}\,0}$ and $\eta_{\mathrm{th}\,0}$ are the threshold current and the differential efficiency of the LCC without allowance for heating of the LD active region and T_I and T_P are the characteristic temperatures for the threshold pump current and the LCC efficiency.

The calculated dependences of CVCs and LCCs on the pump current at different heat-sink temperatures shown in Fig. 1 by dashed curves satisfactorily coincide with the experimental curves.

The formula for heating of the LD active region can be written in the form

$$\Delta T_{\mathrm{LD}}(I, P, \Delta T) = R_{T_0}\left(\frac{T_0 + \Delta T_{\mathrm{LD}}(I, P, \Delta T)}{T_0}\right)^k \times (U(I, \Delta T_{\mathrm{LD}})I - P) + \Delta T, \quad (7)$$

where k is a constant, R_{T_0} is the thermal resistance at the heat-sink temperature $T_0 = 293$ K and $\Delta T = 0, 10, 20, 30$, and 40 K. Calculation shows that, at a pump current of 15 A, the temperature of the active region exceeds the heat-sink temperature by 37.1 °C in the case of the heat-sink temperature of 20 °C and by 42.7 °C when the heat-sink temperature is 60 °C, i. e., additional heating of the active region at a heat-sink temperature of 60 °C is 5.6 °C.

The best coincidence between the experimental and calculated characteristics is observed at $R_{T_0} = 1.8$ K W^{-1}, $T_I = 54$ K, $T_P = 180$ K, $I_{\mathrm{th}\,0} = 1$ A, $U_{0\,\mathrm{cut}} = 0.79$ V, $R_{\mathrm{d}\,0} = 0.076\ \Omega$, $\mathrm{d}R_1 = 0.038$ A^{-1}, $\mathrm{d}R_2 = 0.0023$ A^{-2}, $\mathrm{d}U_1 = 0.005$ K^{-1}, $\mathrm{d}U_2 = 2.6 \cdot 10^{-6}$ K^{-2}, $\eta_{\mathrm{th}\,0} = 0.4$ W A^{-1}, and $k = 1.3$. Thus, we can conclude that the characteristic temperatures T_I (54 K) and T_P (180 K) are considerably lower than the temperatures obtained in [9] for an LD with a stripe contact width of 3 μm and a cavity length of 1.6 mm ($T_I = 80$ K and $T_P = 280$ K). Therefore, an increase in the width to 100 μm leads to an increase in the pump current by almost an order of magnitude and to a stronger temperature sensitivity of the LD characteristics.

Thus, it is shown that a C-mount LD with a cavity length of 2.6 mm and a mesa-stripe contact width of 100 μm allows one to achieve a cw output power exceeding 4 W at a pump current of 15 A. The output power in the pulsed regime amounted to 20 W at a pulse duration of 100 ns, a repetition rate of 5 kHz, and a pump current not exceeding 80 A. The CVCs, LCCs, and characteristic temperatures of the LDs are calculated.

References

1. Garbuzov D., Xu L., Forrest S.R., et al. *Electron. Lett.*, **32**, 1717 (1996).
2. Golikova E.G., Gorbylev V.A., Davidyuk N.Yu., et al. *Tech. Phys. Lett*., **26**, 225 (2000) [*Pis'ma Zh. Tekh. Fiz*., **26**, 5 (2000)].
3. Boucher J.F., Callaban J.J. *Proc. SPIE*, **8039**, 80390B-1 (2011).
4. Garrod T., Olson D., Klaus M., et al. *Proc. SPIE*, **9002**, 90021F-1 (2014).
5. Gorlachuk P.V., Ryaboshtan Yu.L., Ladugin M.A., et al. *Kvantovaya Elektron.*, **43**, 819 (2013) [*Quantum Electron.*, **43**, 819 (2013)].
6. Marmalyuk A.A., Ryaboshtan Yu.L., Gorlachuk P.V., et al. *Kvantovaya Elektron.*, **47**, 272 (2017) [*Quantum Electron.*, **47**, 272 (2017)].
7. Marmalyuk A.A., Ryaboshtan Yu.L., Gorlachuk P.V., et al. *Kvantovaya Elektron.*, **48**, 197 (2018) [*Quantum Electron.*, **48**, 197 (2018)].
8. Tarasov I.S. *Kvantovaya Elektron.*, **40**, 661 (2010) [*Quantum Electron.*, **40**, 661 (2010)].
9. Gorlachuk P.V., Ivanov A.V., Kurnosov V.D., et al. *Kvantovaya Elektron.*, **48**, 495 (2018) [*Quantum Electron.*, **48**, 495 (2018)].
10. Zory P.S. *Quantum Well Lasers* (San Diego, CA: Academic Press Inc., 1993).
11. Elenkrig B.B., Smetona S., Simmons J.G., et al. *Appl. Phys.*, **87**, 1 (2000).
12. Ivanov A.V., Kurnosov V.D., Kurnosov K.V., et al. *Kvantovaya Elektron.*, **33**, 425 (2003) [*Quantum Electron.*, **33**, 425 (2003)].
13. Kurnosov V.D., Kurnosov K.V. *Kvantovaya Elektron.*, **48**, 807 (2018) [*Quantum Electron.*, **48**, 807 (2018)].
14. Gorlachuk P.V., Ivanov A.V., Kurnosov V.D., et al. *Kvantovaya Elektron.*, **44**, 149 (2014) [*Quantum Electron.*, **44**, 149 (2014)].